JOURNAL OF MATERIALS SCIENCE 6 (1971) 1292–1302

Microstructural Studies on Silicon Nitride

A. G. EVANS*, J. V. SHARP†
Atomic Energy Research Establishment, Harwell, Didcot, Berks., UK

Thin specimens of reaction sintered and hot pressed silicon nitride have been prepared by ion beam thinning and examined in the Harwell million volt microscope. It has been found that reaction sintered material consists of large grains, which are mostly β-Si_3N_4, in a fine grained matrix of α-Si_3N_4. Fibres are frequently observed within the pores, the type of fibre depending on the size of the pore. The hot pressed material consists largely of two types of grain, small angular grains of β-Si_3N_4 and larger irregular grains. There is also some non-crystalline material between the angular grains and there are numerous small unidentified inclusions.

The grains of β-Si_3N_4 generally contain dislocations and examination of these shows that most have a $\langle 0001 \rangle$ Burgers vector. The remaining dislocations appear to be more complex, frequently occurring as multiple images, and have not been unambiguously identified. An analysis of dislocations in β-Si_3N_4 shows that $\langle 0001 \rangle$ dislocations are the most stable and are also likely to be most mobile with $\{10\bar{1}0\}$ as the primary slip plane.

1. Introduction

During the last few years, silicon nitride has been established as a material with many potential high temperature engineering applications [1-3]. The successful exploitation of this material will depend to a large extent on the magnitude and reproducibility of strength that can be achieved via microstructural control. The microstructural features of materials with good mechanical properties are very small [4, 5] (typically 0.5 μm, with some features up to 10 μm) and can only be resolved in any detail by transmission electron microscopy. This paper is concerned with a characterisation of the microstructure of both reaction sintered and hot pressed silicon nitrides by transmission electron microscopy, leading to an examination of more specific aspects of the microstructure particularly those that relate to strength.

The strengths of the reaction sintered and hot pressed silicon nitrides examined in this study are shown in fig. 1. At low temperatures where the strength is temperature independent, it has been shown that fracture occurs by the extension of inherent flaws [7]. The strength is then controlled by the size of the largest inherent flaw and by the fracture surface energy. The fracture surface energy is related to the extent of the plastic flow that can occur around the fracture initiating flaw [4, 8], which may in turn be determined by the distribution of second phase material in the vicinity of the crack tip. A more detailed understanding of low temperature strength requires, therefore, some information about the modes of plastic flow in silicon nitride and about the distribution of second phase materials. At high temperatures where the

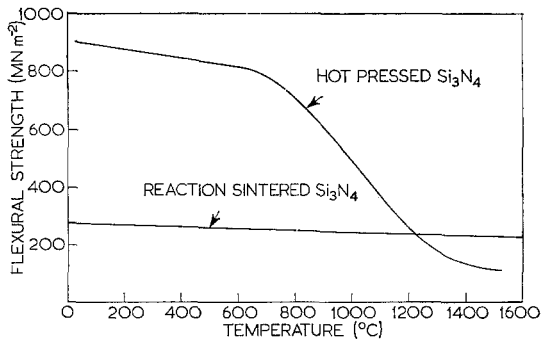

Figure 1 The temperature dependence of the strength of hot-pressed [6] and reaction sintered [5] silicon nitrides.

*Materials Development Division
†Metallurgy Division

strength decreases, fracture is due to the generation of flaws by plastic flow (hot pressed material [6]) and/or a reduction in fracture surface energy due to plastic flow [7]. The strength is thus controlled by plasticity in the second phase material and/or dislocation motion within the silicon nitride. Transmission electron microscopy may assist, therefore, in the understanding of high as well as low temperature strength by identifying the modes of plastic flow in silicon nitride, through dislocation studies and through an examination of the distribution of second phase material. A complete study of plastic flow processes requires extensive and detailed examination of as-fabricated and deformed silicon nitrides. This paper describes the first part of the more general investigation of plasticity and is concerned primarily with a study of dislocations in as-fabricated silicon nitrides.

2. Experimental

Electron transparent sections of various silicon nitrides have been prepared from bulk material by a combination of mechanical grinding and ion beam thinning.

The bulk material was glued to a glass backing plate and ground mechanically to a thickness of < 50 μm. Electron microscope grids (3 mm diameter) containing a slot 2 × 1 mm were then glued to a thin region of the remaining material, care being taken to ensure that the glue did not penetrate the material within the slot. The grid and the thin section contained within it were then separated from the glass backing plate. The grid was essential for mechanical support of the thin section, both during subsequent thinning and for handling purposes.

The final thinning was carried out by ion beam machining, using argon ions with energies of $\sim$ 5 kV. The specimen was rotated at a speed of $\sim$ 3 rev/min, inclined at an angle of $\sim$ 25° to the ion beams. The thinning rate was relatively slow, $\sim$ 1 μm/h. When suitably thin, the specimen and grid were removed from the ion beam machine and coated lightly with carbon on both sides to minimise charging effects. Specimens have been examined mainly at 1 MV on the Harwell EM7 electron microscope, although a small amount of microscopy has been carried out on a 100 kV microscope. High voltages have a particular advantage in this work because it is difficult to produce large thin regions transparent at 100 kV particularly from the lower density reaction sintered material; specimens with larger thin regions were more easily obtained from the dense hot pressed material.

3. Crystallography

Two different forms of silicon nitride have been identified, α and β. Reaction sintered material contains both forms; hot pressed material contains mostly β-Si_3N_4. The α phase is hexagonal with $a = 7.75$Å and $c = 5.62$Å, $c/a = 0.725$; the space group is P31c (C^4_{3v}) with 6 Si in 6(c) at ($x = 0.0724$, $y = 0.5013$, $z = 0.6462$), 6 Si in 6(c) at (0.2554, 0.1673, 0.4509), 6N in 6(c) at (0.6331, 0.5936, 0.4001), 6N in 6(c) at (0.3210, 0.3103, 0.6701), 2N in 2(b) at (0.3333, 0.6667, 0.615) and 2N in 2(a) at (0.0000, 0.0000, 0.385). Some of the nitrogen in 6(c) is often replaced by oxygen with corresponding vacancies in 2(a) [9]. The β phase is also hexagonal with $a = 7.61$Å and $c = 2.91$Å, $c/a = 0.383$; the space group is $P6_3/m$ (C^2_{6h}) with 6 Si in 6(h) at (0.172, − 0.231, 0.250), 6N in 6(h) at (0.333, 0.033, 0.250) and 2N in 2(c) at (0.333), 0.667, 0.250). Interplanar spacings and angles have been calculated for a wide range of planes for both phases [10]. Structure factors have also been determined for the same range of planes [10]. These have then been combined to produce electron diffraction patterns for all combinations of the eight planes with the largest spacings [10]. It is apparent from these that a large proportion of the α and β patterns are very similar and careful diffraction experiments are needed to distinguish the two phases.

Some patterns can be identified immediately as α, i.e. those giving interplanar spacings of 5.6Å or 4.3Å corresponding to (0001) – which may occur due to double diffraction – and $(10\bar{1}1)$ respectively, because there are no similar spacings in the β structure. Conversely, the two phases cannot be distinguished from the $\langle 0001 \rangle$ pattern because the spacings are so similar for α and β-Si_3N_4 (although it may be possible to separate the patterns on an intensity basis [10]). For other orientations, the interplanar spacings and angles cannot be determined absolutely, with an accuracy that is sufficient for an unequivocal identification, unless a pattern from a standard material is obtained on the same film. However, the ratio of the spacings between two types of plane on the same pattern can be obtained with greater accuracy (especially with the million volt microscope) and this is sufficient for the identification of many other low index

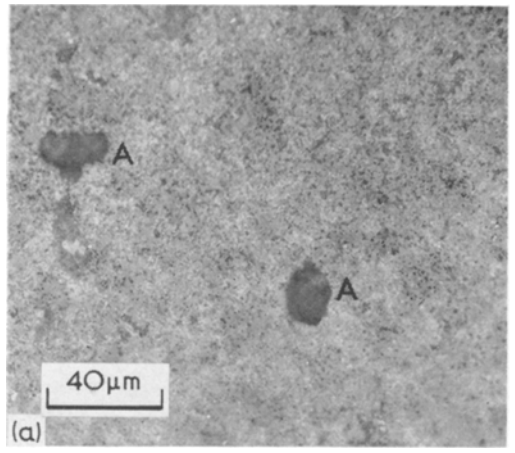

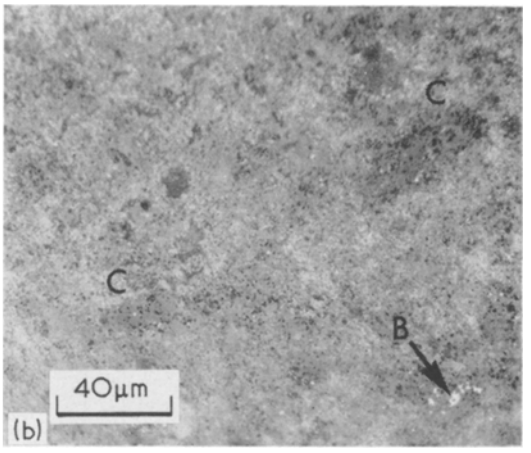

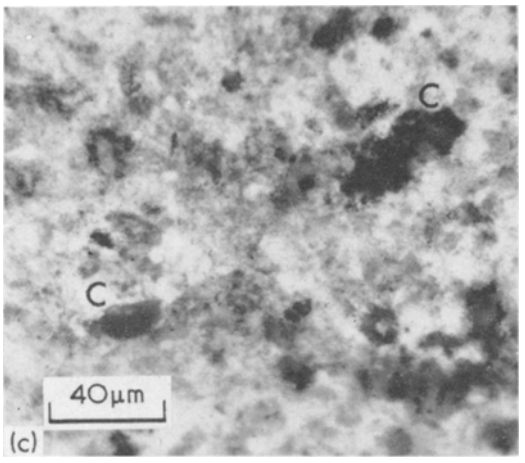

Figure 2 Optical micrographs of vibro-polished reaction sintered silicon nitride. (*a*) Normal reflected light, showing large pores A. (*b*) Normal reflected light, showing the fine porosity (dark regions) and some silicon grains, B. (*c*) Polarised reflected light, showing the silicon nitride grain structure (same area as (*b*)). The dark areas are individual grains, the largest grains occur at C. These areas are also apparent in (*b*) as dark grey regions.

patterns, because the interplanar ratios for any two similar patterns in α or β-Si_3N_4 usually differ by $> 2\%$.

4. Microstructure

4.1. Reaction Sintered Material

Specimens have been prepared by heating compacted silicon in a nitrogen atmosphere in two stages, 60 h at 1350°C followed by 24 h at 1450°C. X-ray analysis has shown that this material consists of 60% α phase, $\sim$ 40% β and $\sim$ 2% unreacted silicon. Optical reflected light microscopy of specimens prepared by vibro-polishing (with γ-alumina powder) shows that the material contains substantial porosity (figs. 2a and b) and some small grains of silicon (fig. 2b). Most of the pores are small, < 1 μm diameter, but some are larger, up to 25 μm long (fig. 2a). An examination of the same areas using polarised light reveals the grain structure of the material (fig. 2c). Most of the grains are small but some larger ones (up to 20 μm long) are also apparent, often occurring as clusters within the fine grained matrix.

Electron microscopy of this material shows large individual grains up to $\sim$ 5 μm in diameter in a background of fine grained material, fig. 3. In some regions there are several large grains close together, extending across $\sim$ 10 μm. These are presumably large grains of the type seen in figs. 2b and c. Many large grains have been investigated and low order diffraction patterns

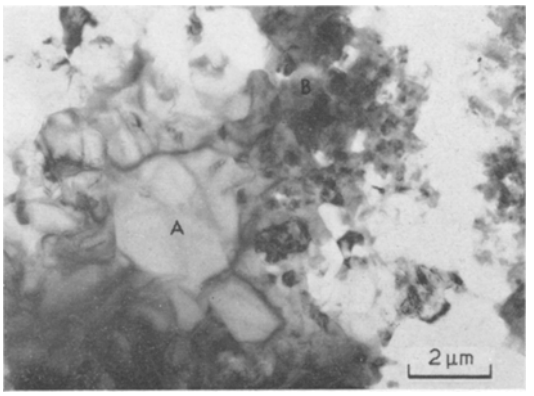

Figure 3 Transmission electron micrograph of a reaction sintered specimen showing coarse grains A in a fine grained matrix B.

Figure 4 Ring diffraction pattern from fine grained matrix (mainly α-phase).

obtained showing that these are mainly β-Si_3N_4. Grains in the background structure, fig. 3, mostly have sizes of a few thousand Å and diffraction patterns from these regions show rings with diameters fitting the α phase, fig. 4. These patterns show that there is no strong preferred orientation of the α grains in the background structure. Larger individual α grains up to ~ 1 μm in size have also been identified fig. 5, and these are generally featureless in contrast to the β grains which frequently contain dislocations.

In some regions the background matte consists mainly of fibres or needles, figs. 6a and b. These needles have also been seen using scanning electron microscopy and form within the pores. Fibres within the largest pores are normally long and narrow, 0.05 μm diameter (fig. 6a). Fibres within the smaller pores are relatively coarse (fig. 6b), up to 0.2μm in diameter, and many have a dark core region. This is thought to be the original fibre formed during the initial stages of nitriding, onto which has grown further silicon nitride during the later stages of the nitriding process. The structure of these needles has so far not been identified by electron microscopy but

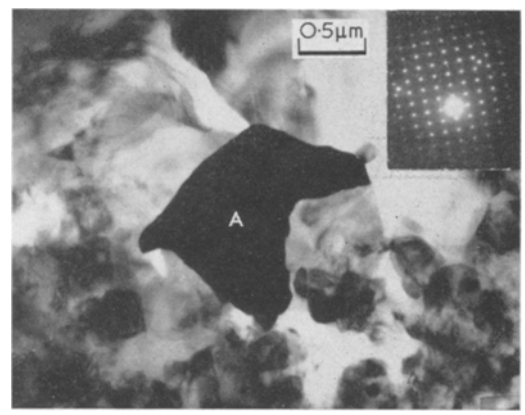

Figure 5 Large featureless grain (A) of α-Si_3N_4 in a reaction sintered specimen. A diffraction pattern from this grain is also shown.

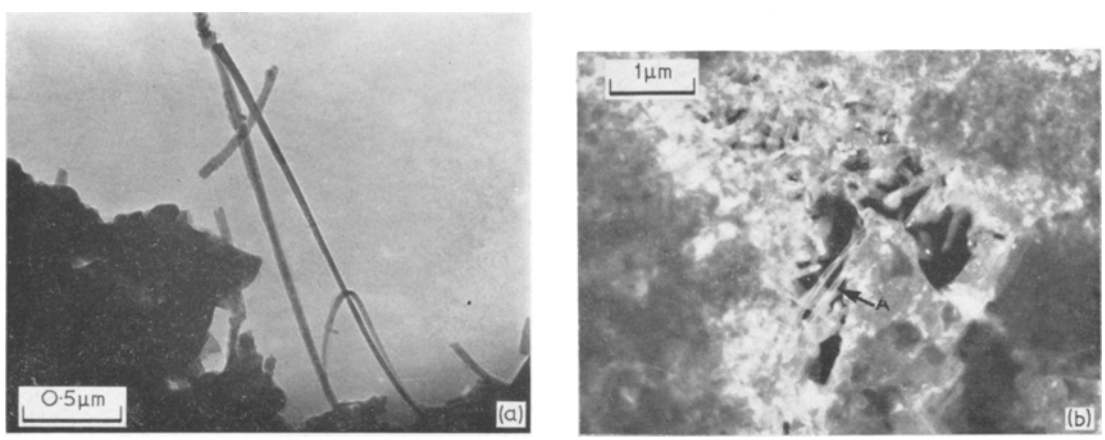

Figure 6 Transmission electron micrographs of fibres in reaction sintered specimens, (a) shows fine fibres at the edge of large pore, (b) shows coarse fibres in a smaller pore. Dark core regions (A) are visible in the coarse fibres.

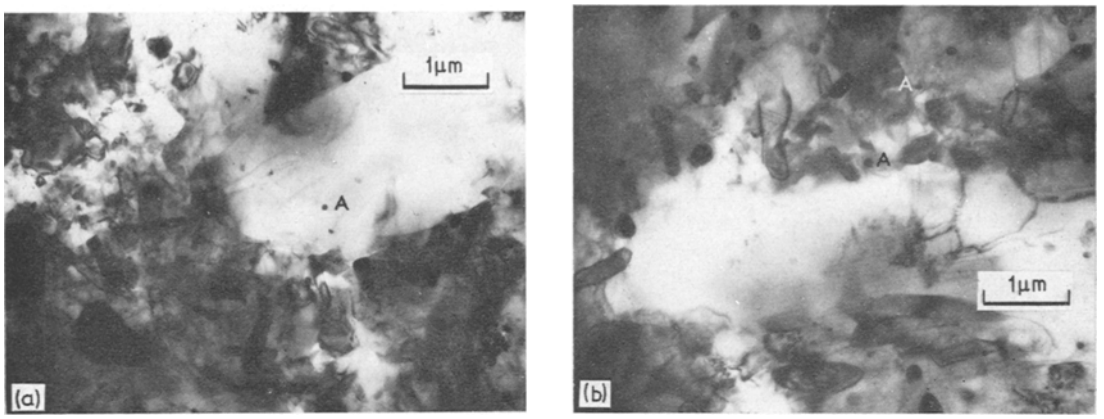

Figure 7 Hot pressed silicon nitride showing small acicular grains and large single grains. Small inclusions (A) are visible in the large grain in (*a*) and in both types of grain in (*b*). The large grains also contain dislocations.

X-ray studies of silicon nitride fibres suggests that they are of the α phase.

No evidence using the electron microscope has so far been found in this reaction sintered material for the presence of unreacted silicon either as individual grains or contributing to a diffraction pattern.

Small scale inter-granular pores have been observed in the background α material by electron microscopy but it is not clear whether these are a real part of the structure or places where individual small grains have dropped out. Large cavities similar in size to those observed using optical microscopy are also visible, often close to large β grains. Where these contain fibres it is evident that they are the pores in the original structure, but cavities without fibres may be the result of preferential ion thinning or the result of large grains disappearing during handling.

4.2. Hot Pressed Silicon Nitride

Specimens obtained from J. Lucas Ltd have been prepared by hot pressing silicon nitride powder (90% α and 10% β) with $\sim$ 5% MgO at 1800°C. An X-ray analysis of the pressed material shows that 80% of the crystalline material is β-Si_3N_4 with the remainder consisting of roughly equal proportions of α-Si_3N_4, silicon carbide and carbon with a small amount of an unidentified phase (probably silicate).

Electron microscopy of these specimens shows two main features (figs. 7a and b). Arrays of small angular (often acicular) grains varying in length from 0.1 to 2 μm and some larger irregular grains up to 8 μm in length.

The smaller angular grains sometimes contain small inclusions, $\sim$ 0.1 μm diameter (fig. 7b). Diffraction patterns from these grains have all been identified as β-Si_3N_4. There are also some areas within the fine grained region which are thought to be non-crystalline, as they do not vary in intensity as the specimen is tilted. These areas lie between certain adjacent grains (fig. 8) and are small ($\sim$0.2 μm across). They are therefore too small for selected area diffraction to confirm their non-crystalline structure.

The larger irregular grains also contain small inclusions (fig. 7*a*) and frequently contain dislocations (fig. 7*b*). Some grains also show arrays of dislocation tangles (fig. 9), indicating that extensive plastic deformation of the grains

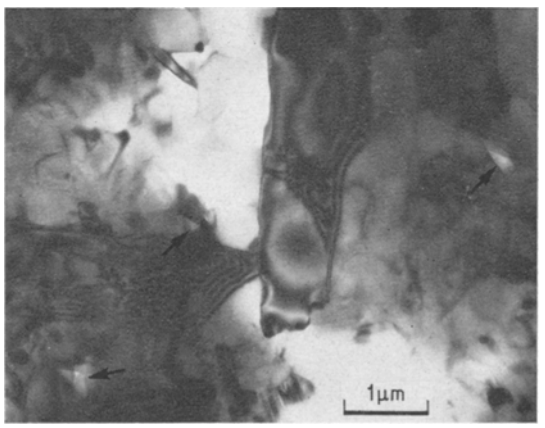

Figure 8 Hot pressed material showing non-crystalline areas (arrowed), as well as a large grain of the type seen in fig. 7.

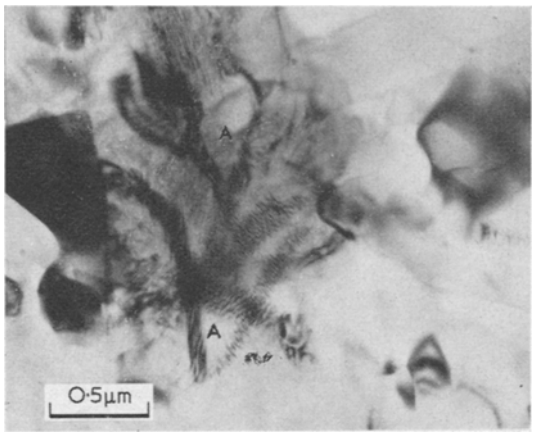

Figure 9 Dislocation tangles (A) in hot pressed silicon nitride.

has occurred at some stage during fabrication. Diffraction patterns from four large grains (two containing dislocation tangles) have again been identified as β-Si_3N_4. None of the other phases present have yet been identified, although at least one of these phases presumably occurs as the small inclusions.

5. Dislocations in Silicon Nitride

The microstructural examinations (section 4) revealed dislocations in most of the larger β-Si_3N_4 grains and in a few of the larger α grains. A more detailed study of the nature of the dislocations has been undertaken for the dislocations in β-Si_3N_4.

5.1. Dislocation Observations

Two types of dislocation have been observed. Both occur in the large grain in figs. 10a and b. Most of the dislocations disappear when the specimen is tilted to obtain a $\langle 11\bar{2}0\rangle$ reflection, fig. 10b. The same dislocations are out of contrast for $\langle 12\bar{3}0\rangle$ and $\langle 10\bar{1}0\rangle$ reflections, thus identifying the Burgers vector as $\langle 0001\rangle$, i.e. c-axis. It is also noted that these dislocations are mainly in screw orientation.

The remaining dislocations disappear with a $\langle 10\bar{1}1\rangle$ reflection operating and in this reflection the $\langle 0001\rangle$ dislocations are in contrast. The Burgers vector of these dislocations is probably of the type **a** or (**c** + **a**) although this has not so far been confirmed. The image of these particular dislocations has been noted to be more complex than that of $\langle 0001\rangle$ type dislocations. In many cases multiple dislocation images are obtained for both bright and dark field conditions although no fringes or bands have been identified between the images. The multiple images may be due to the splitting of the dislocations into partials or possibly the result of many beam

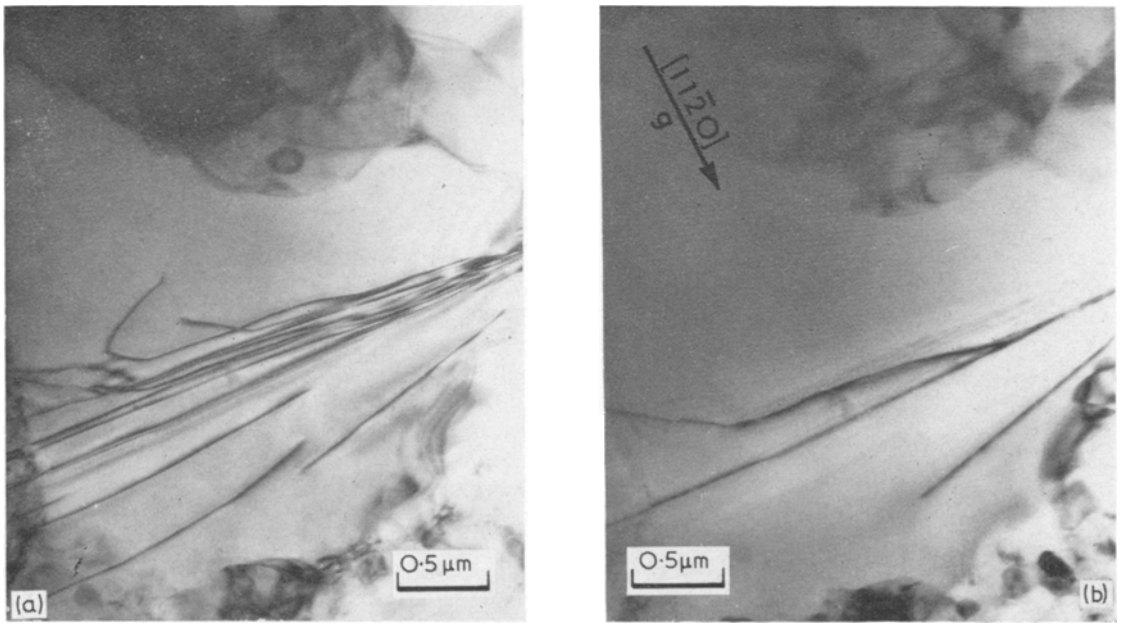

Figure 10 (*a*) Long dislocations in a large β-grain in a reaction sintered specimen. (*b*) Same area showing one set of dislocations out of contrast, $\mathbf{g} = [11\bar{2}0]$.

diffraction effects at high voltages. Unfortunately the grains containing these long dislocations are not normally transparent at 100 kV and it has not been possible so far to obtain two beam images. This is being investigated further and will be dealt with in a subsequent paper.

5.2. Analysis of Dislocations in β-Si_3N_4

5.2.1. Dislocation stability

The strain energy of a dislocation can be conveniently separated into two parts, that due to the small displacements outside the core (U_1), where elasticity theory can be applied, and that due to the large displacements within the core (U_2). U_1 is usually the major contribution and is proportional to $\mathbf{b}^2$ (**b** Burgers vector). The most stable dislocations then have the minimum values of **b**. In some covalent or ionic materials, however, U_2 is very sensitive to the direction of **b** and variations in U_2 can then be more important than variations in U_1. To determine the most stable dislocations in β-Si_3N_4, which has a 70% covalent and 30% ionic bonding [11] the contributions due to both U_1 and U_2 should be considered.

Dislocations with the two smallest values of U_1 have Burgers vectors of the type $\langle 0001 \rangle$ (*c*-axis) and $\frac{1}{3}\langle 11\bar{2}0 \rangle$ (*a*-axis). The Burgers vector for the *c*-axis dislocations is 2.91Å and for the *a*-axis dislocations is 7.60Å. U_1 is therefore more than five times larger for the *a*-axis dislocations than *c*-axis dislocations. There are, however, a number of ways in which the former may dissociate into partials to reduce U_1, e.g. $AC \rightarrow AB + BC$ and $AC \rightarrow AB' + B'B + BC$ (fig. 11). The minimum value for U_1 that can be achieved by dissociation is still more than twice that for the *c*-axis dislocation (with an additional energy term due to the associated stacking fault). Unless the core energy of the $\langle 0001 \rangle$ dislocations is very much larger than that for $\frac{1}{3}\langle 11\bar{2}0 \rangle$ dislocations the most stable dislocations will have Burgers vectors of the type $\langle 0001 \rangle$.

The relative core structures of *c* and *a*-axis dislocations may be assessed from a $[10\bar{1}0]$ projection (fig. 11). Firstly, it is noted that the core of the *c*-axis dislocation contains fewer ions (bonds) than the *a*-axis dislocation. An edge dislocation with a $\langle 0001 \rangle$ Burgers vector has two extra half planes and an edge dislocation with $\frac{1}{3}\langle 11\bar{2}0 \rangle$ vector has four extra half planes (two of which are serrated). More ions are therefore subjected to relatively large displacements in *a*-axis dislocations than in *c*-axis dislocations and U_2 is likely to be larger for *a*-axis dislocations.

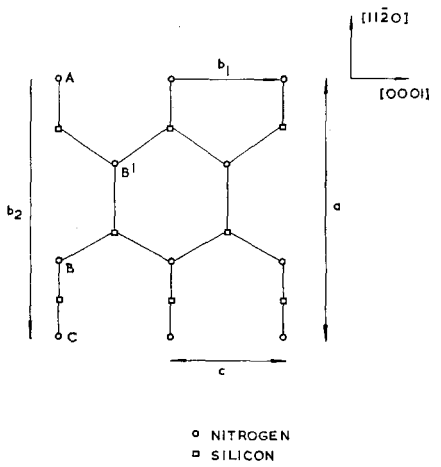

Figure 11 A $\{10\bar{1}0\}$ projection of β-Si_3N_4 showing two possible Burgers vectors, $[0001] - \mathbf{b}_1$ (*c*-axis), and $[11\bar{2}0] - \mathbf{b}_2$ (*a*-axis).

The most stable dislocations thus have Burgers vectors of the type $\langle 0001 \rangle$. This is consistent with the high densities of $\langle 0001 \rangle$ dislocations observed experimentally, and the relatively small proportion of other dislocations. There are no other hexagonal structures in which $\langle 0001 \rangle$ has been analysed as the most stable Burgers vector. In fact only one previous observation of dislocations (other than loops) with this Burgers vector is known to the authors, and this is in beryllium at high temperatures [12].

5.2.2. Dislocation mobility

The simple Peierls model often gives a first approximation for the slip system containing the most mobile dislocations—the primary slip system. This model predicts that the stress to move dislocations is proportional to $\exp(-2\pi d/\mathbf{b})$, where d is the spacing between the slip planes. The most mobile dislocations will generally have the smallest Burgers vector therefore and hence, for β-Si_3N_4, there will be a strong preference for slip on systems with a $\langle 0001 \rangle$ Burgers vector. The primary slip plane is more difficult to predict because the interplanar spacing, d, has little significance in a complex structure such as β-Si_3N_4. The simple Peierls model is inadequate and a more detailed consideration of the structural changes that occur during dislocation movement is required.

The major consideration in this mainly covalently bonded material will be the relative distortions of the covalent bonds. A secondary consideration is the change in charge distribution due to the partly ionic nature of the bond. The favoured slip plane is assessed on this basis from an examination of the structure along {0001} planes (fig. 12).

The maximum energy position during slip is the mid-translation distance, i.e. at **b**/2. The system with the minimum energy at this position will be the primary slip plane. Consider, therefore, in fig. 12, translations of $c/2$ perpendicular to the plane of the paper on opposite sides of the proposed slip plane. Firstly, it is evident that planes of the type A_2A_2' are not favourable because they require large distortions of the bonds between atoms of the type XX'. Planes of the type A_1A_1' will be preferred where the largest bond distortions, between atoms X and X″, are relatively small, $< 30°$. A considerable number of planes which do not contain XX' bonds may be selected, each one requiring identical bond distortions, of XX″ type bonds. The basis for selection of the most likely slip plane is not, therefore, the extent of the bond distortion but the number of bonds that require distortion per unit length of dislocation. This may be determined from fig. 13. The three types of plane with the smallest number of bond distortions for a given dislocation length are $\{10\bar{1}0\}$, $\{11\bar{2}0\}$ and $\{12\bar{3}0\}$. For a $\{10\bar{1}0\}$ slip plane, the smallest number of bond distortions, e.g. along AA', is seven in a length $3a$ of dislocation, a mean spacing between bonds of $\sim$ 3.4Å. For a $\{11\bar{2}0\}$ slip plane, e.g. CC', the mean spacing between bonds is 2.9Å. For a $\{12\bar{3}0\}$ plane, e.g. BB', the mean spacing between bonds is 3.0Å. There will thus be a strong tendency for slip to occur at the lowest applied shear stress on $\{10\bar{1}0\}$ planes, unless the ion displacements due to slip on other planes require a substantially smaller increase in electrostatic energy.

The electrostatic interaction between two ions is proportional to $1/r^2$, where r is the separation of the ions. The major part of the change in electrostatic energy after an ion displacement is due to the interactions with nearest and next nearest neighbour ions. An assessement of the change in electrostatic energy due to dislocation motion may therefore be obtained by considering the interactions between the nearest and next nearest ions across the slip plane. The relative ion displacements due to slip may be visualised in fig. 14. The three major interaction changes that occur during a displacement to the mid-translation position are: (*a*) nitrogen ions of type α with nearest neighbour (bonded) silicon ions of type β_1, (*b*) nitrogen ions with the three other nitrogen ions bonded to the same silicon ion, γ_1 and β_2 (one in plane of paper and one c above or below plane of paper) and (*c*) nitrogen ions δ_2

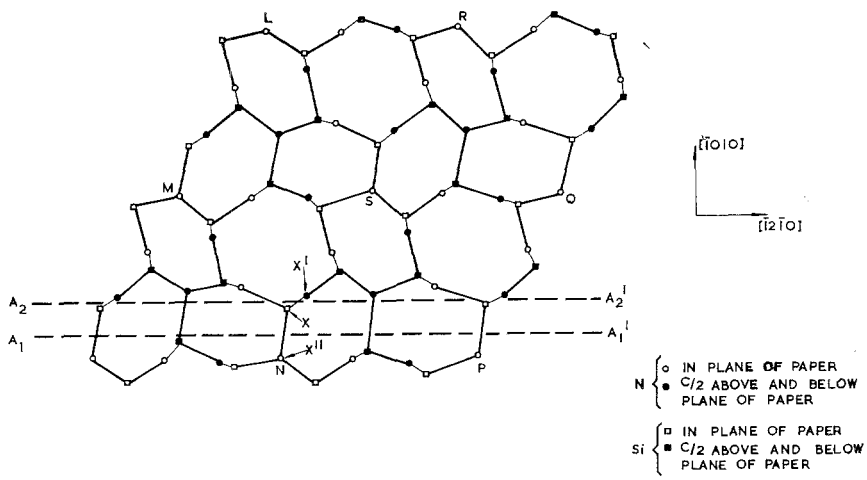

Figure 12 A {0001} projection of β-Si_3N_4. LMNPQR are the corners of the hexagonal unit cell with S as the centre. A_2A_2' is a plane passing through bonds inclined to the basal plane; A_1A_1' is chosen to pass through bonds lying in the basal plane only. The planes are represented by straight lines for convenience, although in practice they pass midway between each pair of atoms lying on opposite sides of the plane, e.g. atoms X'X″, and hence are serrated.

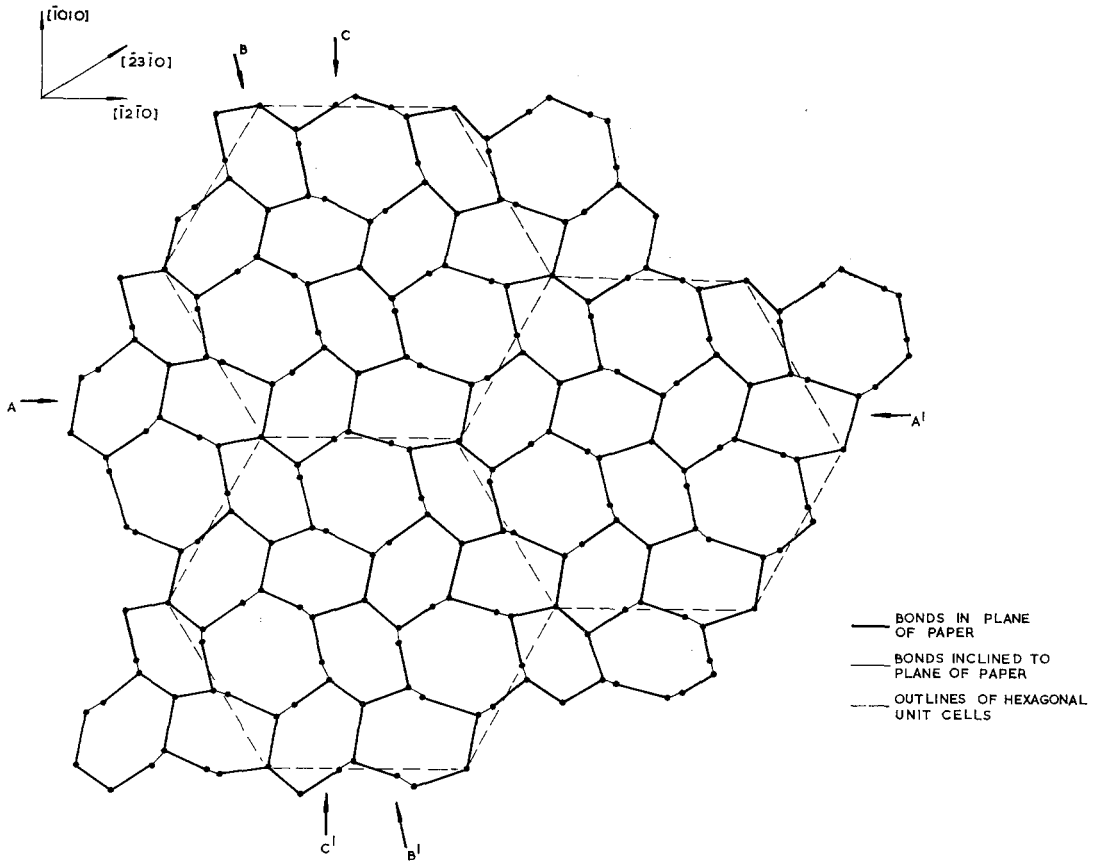

Figure 13 A {0001} projection of β-Si_3N_4 showing the covalent bonding; AA′, BB′, CC′ are three possible slip planes corresponding to $\{10\bar{1}0\}$, $\{12\bar{3}0\}$ and $\{11\bar{2}0\}$ respectively.

(or γ_1) with next nearest neighbour silicon ions γ_2 (or δ_1). Displacements of type (*a*) increase the electrostatic energy (by ΔV_1) because unlike ions are moved farther apart (from 1.8 to 2.3Å): displacements (*b*) reduce the electrostatic energy because an α ion is moved farther from like ions γ_1 and also from one β_2 ion but closer to the other β_2 ion (the net energy reduction is $\sim 0.1\ \Delta V_1$): displacements (*c*) increase the electrostatic energy by moving unlike ions farther apart (the energy increase is $\sim 0.2\ \Delta V_1$). All other interactions give energy changes $< 0.05\ \Delta V_1$ and tend to cancel out; they are not likely to be important. An examination of these major interactions across slip planes AA′ BB′ and CC′ shows that there is an increase in electrostatic energy due to slip on each system. This increase is marginally smaller for AA′ than BB′ or CC′.

It may be concluded, therefore, that the primary slip plane is likely to be $\{10\bar{1}0\}$ with $\{11\bar{2}0\}$ and $\{12\bar{3}0\}$ as potential secondary systems.

6. Discussion

6.1. Microstructure

6.1.1. Reaction sintered material

The development of the observed microstructure may be understood qualitatively in terms of the reaction sintering process. During the initial reaction sintering stage, below the melting temperature of silicon, X-ray studies have shown that the silicon nitride formed is predominantly α-Si_3N_4. The electron microscope studies show that most of the α-Si_3N_4 in the final structure occurs as the fine grained matrix. It follows therefore that the reactions occurring during the initial stage lead primarily to the formation of the matrix regions.

When sintering commences fine fibres (fig. 6a) start to form within the pores of the silicon compact [4]. The fibres within the smaller pores

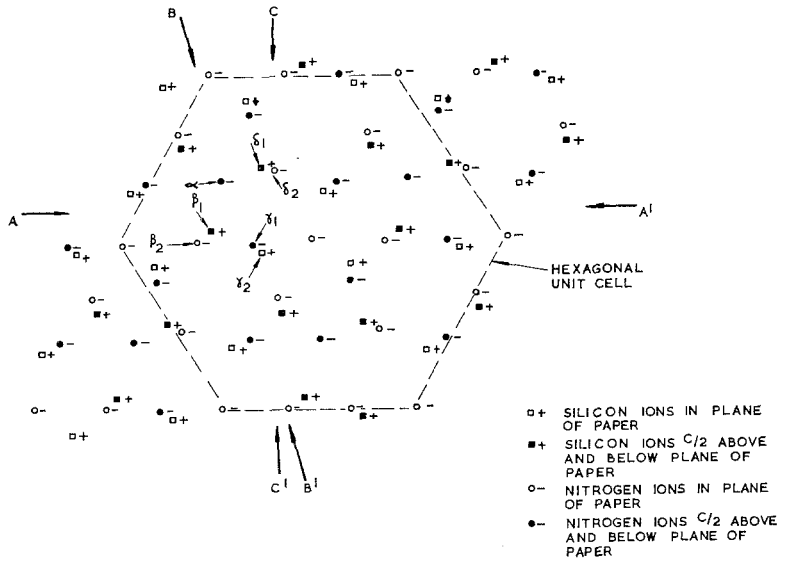

Figure 14 A {0001} projection of β-Si_3N_4 showing the ion positions; AA′, BB′ and CC′ are the same as in fig. 13.

then act as nucleation sites for further deposition of silicon nitride and the thickness of the fibres increases to form the thick fibres of irregular shape shown in fig. 6b. In regions where the fibre density is relatively high the fibres probably grow together and, after subsequent sintering, generate the fine grained matrix. At this stage most of the reaction has occurred by vapour/vapour or solid/vapour processes.

During the final reaction sintering stage above the silicon melting temperature most of the silicon nitride forms as β-Si_3N_4. It is during this stage, therefore that the coarse β grains form by a liquid/vapour process. However, reaction sintering at this temperature does not produce coarse β grains exclusively. The growth of fibres can still proceed as in the previous stages and also, where molten silicon is not retained by a nitride shell it can run into the matrix [4] and will increase the density of the matrix forming some fine grains of α or β-Si_3N_4.

6.1.2. Hot-pressed material

The microstructure of hot pressed silicon nitride may also be described in terms of the fabrication process. The material is produced by hot pressing mostly α-Si_3N_4 powder with a small quantity of MgO. X-ray studies show that, during hot pressing, the α-Si_3N_4 converts mostly to β-Si_3N_4 and that the MgO reacts with some Si_3N_4 to form a non-crystalline silicate phase. The angular grains observed in the electron microscope are mostly smaller than the particles in the original powder [5] and presumably these form from the α-Si_3N_4 particles, via a solid state transformation. The larger irregular β grains are similar in size to the original powder particles. These particles presumably remain throughout the hot pressing process. Some of the particles are heavily deformed during pressing. This suggests that extensive dislocation motion can occur in β-Si_3N_4 at $\sim$ 1800°C in grains of the appropriate orientation.

6.2. Strength

It has been shown that most of the dislocations in as-fabricated β-Si_3N_4 have $\langle 0001 \rangle$ Burgers vectors and these are likely to move initially on $\{10\bar{1}0\}$ slip planes. Whether these dislocations influence the strength of silicon nitride will be determined by the relative values of the stress to move dislocations and the stress to extend the inherent flaws [7]. There are indications from the hot pressed material that extensive dislocation motion can occur at least at $\sim$ 1800°C. Dislocation initiated fracture must, therefore, be considered as a possible high temperature failure mechanism. Dislocation motion is also likely to occur around crack tips at lower temperatures, thereby having an effect on low temperature strength. Work is planned on deformed material and this will enable the relationships between

dislocation motion and strength to be examined in more detail.

7. Conclusions

(1) Thin specimens of reaction sintered and hot pressed silicon nitride have been prepared by ion beam thinning. Large thin areas are readily obtained from hot pressed material; a less uniform, but satisfactory, thinning is achieved with the reaction sintered material.

(2) The microstructure of reaction sintered silicon nitride consists of large grains (up to 5 μm long) of mostly β-Si_3N_4 and a fine grained matrix of α-Si_3N_4. The β grains generally contain dislocations. The pores frequently contain fibres; fibres within the large pores are long and narrow, whereas fibres in small pores are coarser and contain a narrow core. The matrix and fibres form primarily whilst nitriding below the silicon melting temperature. The β grains form mostly above the silicon melting temperature.

(3) The microstructure of hot pressed silicon nitride consists mostly of small angular grains of β-Si_3N_4 with some larger irregular grains; only a few larger grains have been identified but all of these have been β-phase. Some small non-crystalline regions are observed between certain of the small angular grains. No other phases have yet been identified although one phase occurs as numerous small inclusions. Some of the large irregular grains are probably the β particles from the original powder; the smaller angular grains are transformed from α particles during hot pressing.

(4) Dislocations have been studied in β-Si_3N_4. Most of the observed dislocations have a $\langle 0001 \rangle$ Burgers vector; the remainder have not yet been identified. This is the first known observation of primary dislocations with a c-axis Burgers vector.

(5) An analysis of dislocations in β-Si_3N_4 shows that the most stable dislocations are likely to have a $\langle 0001 \rangle$ Burgers vector, consistent with the dislocation observations. These dislocations are also likely to be the most mobile with $\{10\bar{1}0\}$ as the primary slip plane. Dislocations moving on this system may limit the high temperature strength of various silicon nitrides.

Acknowledgements

The authors wish to thank Dr R. W. Davidge for many valuable discussions and for comments on the original manuscript, and Mr C. W. A. Maskell for assistance with the design and operation of the ion beam thinning machine.

References

1. N. L. PARR and E. R. W. MAY, *Proc. Brit. Ceram. Soc.* 7 (1967) 81.
2. D. J. GODFREY, Metals and Materials (1968) 305.
3. D. E. STODDART and R. P. GRAHAM, Materials Towards the 70's (1969) 20.
4. A. G. EVANS and R. W. DAVIDGE, *J. Mater. Sci.* **5** (1970) 314.
5. R. J. LUMBY and R. F. COE, *Proc. Brit. Ceram. Soc.* **15** (1970) 91.
6. A. G. EVANS, unpublished results on material supplied by J. Lucas Ltd.
7. R. W. DAVIDGE and A. G. EVANS, *Mater. Sci. Eng.* **6** (1970) 281.
8. A. G. EVANS, *Phil. Mag.*, **22** (1970) 841.
9. S. WILD, P. GRIEVESON, K. H. JACK, and M. S. LATIMER, *Special Ceramics*, **5** (1971) to be published.
10. A. G. EVANS, J. V. SHARP, and B. HUDSON, to be published.
11. D. S. THOMPSON and P. L. PRATT, *Sci. Ceramics*, **3** (1966) 33.
12. R. I. GARBER, I. A. GINDIN, and Y. V. SHUBIN, *Sov. Phys. Solid State*, **3** (1961) 832.

Received 22nd June and accepted 28 June 1971.